Towards osteogenic and bactericidal nanopatterns?

Widyaratih, Dwisetya S.; Hagedoorn, Peter Leon; Otten, Linda G.; Ganjian, Mahya; Tümer, Nazlı; Apachitei, Iulian; Hagen, Cornelis W.; Fratila-Apachitei, Lidy E.; Zadpoor, Amir A.

DOI
10.1088/1361-6528/ab0a3a

Publication date
2019

Document Version
Final published version

Published in
Nanotechnology

LETTER

Towards osteogenic and bactericidal nanopatterns?

To cite this article: Dwisetya S Widyaratih *et al* 2019 *Nanotechnology* **30** 20LT01

IOP Publishing Letters
Nanotechnology
Nanotechnology 30 (2019) 20LT01 (9pp) https://doi.org/10.1088/1361-6528/ab0a3a

Letter

Towards osteogenic and bactericidal nanopatterns?

Dwisetya S Widyaratih[1], Peter-Leon Hagedoorn[2], Linda G Otten[2], Mahya Ganjian[1], Nazlı Tümer[1], Iulian Apachitei[1], Cornelis W Hagen[3], Lidy E Fratila-Apachitei[1,4] and Amir A Zadpoor[1,4]

[1] Department of Biomechanical Engineering, Faculty of Mechanical, Maritime, and Materials Engineering, Delft University of Technology (TU Delft), Mekelweg 2, Delft 2628CD, The Netherlands
[2] Department of Biotechnology, Faculty of Applied Sciences, Delft University of Technology (TU Delft), van der Maasweg 9, Delft 2629HZ, The Netherlands
[3] Department of Imaging Physics, Faculty of Applied Sciences, Delft University of Technology (TU Delft), Lorentzweg 1, Delft 2628CJ, The Netherlands

E-mail: e.l.fratila-apachitei@tudelft.nl

Received 11 January 2019, revised 14 February 2019
Accepted for publication 25 February 2019
Published 11 March 2019

Abstract

Recent discoveries have shown that nanopatterns with feature sizes ⩽100 nm could direct stem cell fate or kill bacteria. These effects could be used to develop orthopedic implants with improved osseointegration and decreased chance of implant-associated infections. The quest for osteogenic and bactericidal nanopatterns is ongoing but no controlled nanopatterns with dual osteogenic and bactericidal functionalities have been found yet. In this study, electron beam induced deposition (EBID) was used for accurate and reproducible decoration of silicon surfaces with four different types of nanopatterns. The features used in the first two nanopatterns (OST1 and OST2) were derived from osteogenic nanopatterns known to induce osteogenic differentiation of stem cells in the absence of osteogenic supplements. Two modifications of these nanopatterns were also included (OST2-SQ, OST2-H90) to study the effects of controlled disorder and lower nanopillar heights. An *E. coli* K-12 strain was used for probing the response of bacteria to the nanopatterns. Three nanopatterns (OST2, OST2-SQ, and OST2-H90) exhibited clear bactericidal behavior as evidenced by severely damaged cells and disrupted formation of extracellular polymeric substance. These findings indicate that controlled nanopatterns with features derived from osteogenic ones can have bactericidal activity and that EBID represents an enabling nanotechnology to achieve (multi)functional nanopatterns for bone implants.

Supplementary material for this article is available online

Keywords: nanopatterns, bactericidal, cells, osteogenic, electron beam induced deposition

(Some figures may appear in colour only in the online journal)

1. Introduction

Nanopatterns with feature sizes ⩽100 nm have been recently discovered to determine stem cell fate [1–4] or kill bacteria [5–7]. The effects of nanopatterns on stem cells go through mechanobiological pathways including regulation of focal adhesions [8, 9]. As for the bactericidal effect, the deformations imposed by the nanopatterns are stipulated to be the main driving mechanisms [5, 7, 10, 11]. Both effects could therefore be seen as mechanical in nature. Regenerative as well as permanent implants could benefit from such effects of

[4] Both authors contributed equally.

nanopatterns to, on the one hand, promote tissue regeneration and, on the other hand, prevent implant-associated infections.

In the case of orthopedic implants, instructive nanopatterns that stimulate differentiation of mesenchymal stem cells (MSCs) towards the osteogenic lineage are of interest. Possible mechanisms by which nanopatterns induce osteogenic differentiation involve interactions at subcellular and molecular levels, and mechanotransduction pathways via integrin clustering, formation of large focal adhesions, and subsequent increase in intracellular tension [2, 12–15]. Relative to chemical triggers, activation of such molecular mechanisms by nanotopographical cues offers the advantage of a stable, better controlled, and safer interface, as well as a faster signal transmission towards the nucleus [16]. As for the antibacterial behavior, specific types of nanopatterns induce deformations in the cell wall [5, 7, 10, 11] that are beyond the allowable limit, thereby causing rupture and deformation-mediated cell death.

Controlled and reproducible nanopatterns that simultaneously instruct MSCs to commit to the osteogenic lineage and exhibit bactericidal effects are the holy grails of nanopattern design for orthopedic implants [17]. The most important research question in this regard is 'what shapes, dimensions, and arrangements of nanopatterns should be used to simultaneously achieve both goals?' To answer this question, we need to systematically study the effects of the above-mentioned parameters on the desired effects. That has never happened before due to the technical challenges associated with accurate and reproducible fabrication of nanopatterns with pre-defined shapes, dimensions, and arrangements. Recently, we have shown how electron beam induced deposition (EBID) could be used for free-form ornamentation of titanium surfaces [18] that are later folded using origami techniques to create 3D lattice structures (the basis for porous orthopedic implants). EBID enables direct (maskless) writing with single digit nanometer resolution by using precursor gas molecules that dissociate under the electron beam on the substrate and form a nano-deposit [19]. We have also demonstrated the accuracy and reproducibility of the nanofeatures (10–100 nm) that make up the free-form ornaments. This makes EBID an ideal technique for such systematic studies.

Here, we used EBID to study the antibacterial behavior of nanopatterns having features derived from osteogenic nanopatterns. These osteogenic nanopatterns have been produced on different materials such as titanium [4, 14] and polymers [15, 20–23] by various methods [2]. Most of the nanopatterns showing *in vitro* osteogenic potential in the absence of osteogenic supplements possess small heights (15–20 nm) [4, 14] or controlled spatial arrangements (namely 50 nm displacement from a square arrangement of 120 nm diameter pits with 300 nm interspace) [2, 12, 15, 20–23]. In addition, nanopillars with heights of 15–20 nm have been recently shown to exhibit osteogenic activity *in vivo*, further confirming the osteogenic potential of such nanopatterns [3]. We therefore focused on both types of above-mentioned nanopatterns: nanopillars with heights of 15–20 nm (OST1) as well as a square arrangement of pillars with diameters of 120–130 nm, 300 nm interspace and controlled disorder (i.e. 50 nm deviation from the square arrangement) (OST2). The study was expanded to include other relevant nanopatterns namely an *ordered* square arrangement of the nanopillars (OST2-SQ) and pillars of lower heights (90 versus 180 nm; OST2-H90). A model strain, namely *Escherichia coli* (*E. coli*) K-12, was used for evaluating the antibacterial effects of all above-mentioned types of nanopatterns.

2. Materials and methods

The nanopillars were grown on silicon wafers using trimethyl (methylcyclopentadienyl)-platinum (IV) ($C_9H_{16}Pt$) precursor molecules in a Nova NanoLab 650 Dual Beam system (FEI, Oregon) (see figure S1 for more details at stacks.iop.org/NANO/30/20LT01/mmedia). The background vacuum of the system was 1.0–3.0 $\times$ 10^{-6} mbar and the EBID process started at 4.0–6.0 $\times$ 10^{-6} mbar. Writing was performed based on a single dot exposure with a 20 kV beam and a current of 2.4 nA. The focused electron beam was controlled by stream files written in MATLAB (see figure S2 for more details). All the conditions used to generate the EBID nanopatterns are summarized in table S1.

Following the patterning process, the precursor gas was pumped out of the system and the patterns were kept in the chamber overnight before imaging using the same system (to avoid deposition of the residual precursor molecules). Top and tilted images of the resulting nanopillars were acquired at various magnifications. The base diameter, height and interspace of the pillars were estimated from tilted SEM images. The diameter was assessed by fitting an ellipse to the base plane whereas the height was determined by measuring the distance between the center of the base plane and the tip of the pillar. The height values were corrected for the tilt angle.

The UV sterilized samples were incubated with *E. coli* K-12 cells (OD_{600} = 0.05) at 37 °C for 18 h (see figure S3 for more details). At least triplicates were cultured for each type of nanopatterns. After the incubation, the samples were rinsed with 0.01 M phosphate-buffered saline (PBS), pH 7.4, fixed, dried and sputter coated with gold for SEM imaging. The samples were imaged with the same Nova NanoLab 650 Dual Beam system using an acceleration voltage of 5 kV and a beam current of 0.4 nA. Top views and tilted images at various angles and magnifications have been acquired for investigating the cells, cell-pattern interface and cell-pillars interface. Using the SEM images, characteristic dimensions of the cells were measured (length and width) together with the cell density (relative to the non-patterned area) and the projected area of the extracellular polymeric substance (EPS). In addition, the ratio of damaged cells was determined for each pattern (see figure S4 for more details). The bacteria were considered damaged if severe deformation (change in shape) occurred (such as wrinkling and completely flat shapes). The same morphological characterization was performed for cells cultured on control surfaces, namely the silicon substrate and the smooth PtC deposit (see figures S5 and S6).

(a)

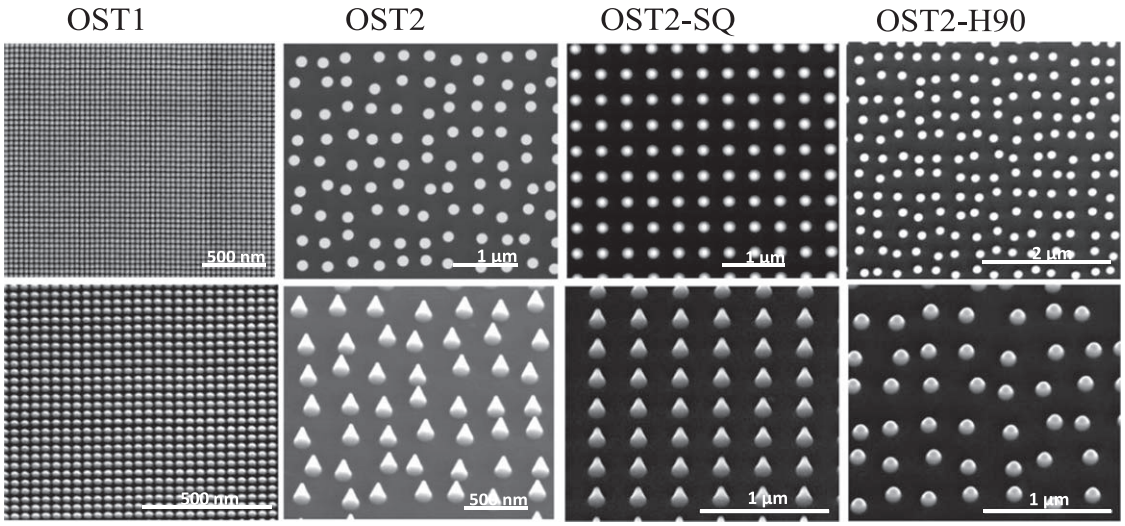

(b)

Nanopattern	Diameter (nm)	Height (nm)	Interspace (nm)	Aspect ratio (Height/Diameter)
OST1	28 ± 1	21 ± 2	40 ± 2	0.75
OST2	122 ± 22	183 ± 9	300 ± 50	1.5
OST2-SQ	124 ± 6	188 ± 9	299 ± 4	1.5
OST2-H90	126 ± 8	94 ± 8	300 ± 50	0.75

Figure 1. (a) Top (first line) and tilted SEM images of the EBID nanopatterns; (b) morphological characteristics of the nanopatterns.

To assess whether the variables including cell length, cell width, EPS area, density and damaged cell ratio significantly varied between the groups (i.e. OST1, OST2, OST2-SQ and OST2-H90), an analysis of variance (ANOVA) was performed. For each variable, the normality of data and the equality of variances between the groups were evaluated using the Shapiro–Wilk and Levene's tests, respectively. The pair-wise comparisons of the groups were realized using either Bonferroni (i.e. p-value >0.05 resulting from Levene's test) or Games-Howell (i.e. p-value <0.05 resulting from Levene's test) post-hoc tests, in case the data for a given variable was normally distributed (i.e. p-value >0.05 resulting from Shapiro–Wilk test). When the normality assumption was violated, the Kruskal–Wallis test followed by the Dunn's post-hoc test was carried out.

3. Results and discussion

The nanopillars grown on silicon wafers using $C_9H_{16}Pt$ precursor molecules exhibited the desired features in terms of the shape, dimensions, and reproducibility (figure 1). The deposits from this precursor typically consist of carbon (ca. 73 at%) with 21.5 at% Pt and some O (ca. 5.5 at%) [24–26]. The Pt:C stoichiometric ratio of the deposit is 1:8 as a result of one Pt–CH_3 bond cleavage and formation of CH_4 and hydrogen under the electron beam [19]. Structurally, the nanopillar is a nanocomposite material with Pt nanocrystals of ca. 1.8–2.1 nm in size incorporated in an amorphous carbon matrix [27, 28].

The response of *E. coli* K-12 was strongly dependent on the type of nanopattern (figures 2, 3). Preliminary experiments on control surfaces, namely silicon wafers and smooth PtC deposits, indicated no toxic effects of the materials on the *E. coli* K-12 cells (figure S5, supplementary document). In addition, the optical density (OD_{600}) of the planktonic cells cultured on silicon wafers and PtC were similar and increased from 0.05 to 1.4 within 18 h.

On the OST1 nanopatterns (figures 2(a)–(d)), the cells could adhere to the surface and kept their physiological morphology, namely the characteristic rod shape with a length of 1.9 ± 0.6 μm and an average width of 570 ± 98 nm (mean ± SD) (figures 3(a), (b)). The cells produced EPS that was visible on the entire cell body as well as on the adjacent nanopatterned surface, following closely the cell body (figures 2(b), (d)). Moreover, no damaged cells were detected on OST1 surfaces (figure 3(d)). However, fewer cells seemed to adhere to the patterned areas as compared to the surrounding non-patterned areas (figure 3(e)). This observation suggests that OST1 may be inhibiting *E. coli* adhesion.

The cells could not easily adhere to the surfaces decorated with OST2 (figures 2(e)–(h)) and their morphology revealed significant changes including presence of cells with extremely large lengths (maximum cell length around 7.0 μm,

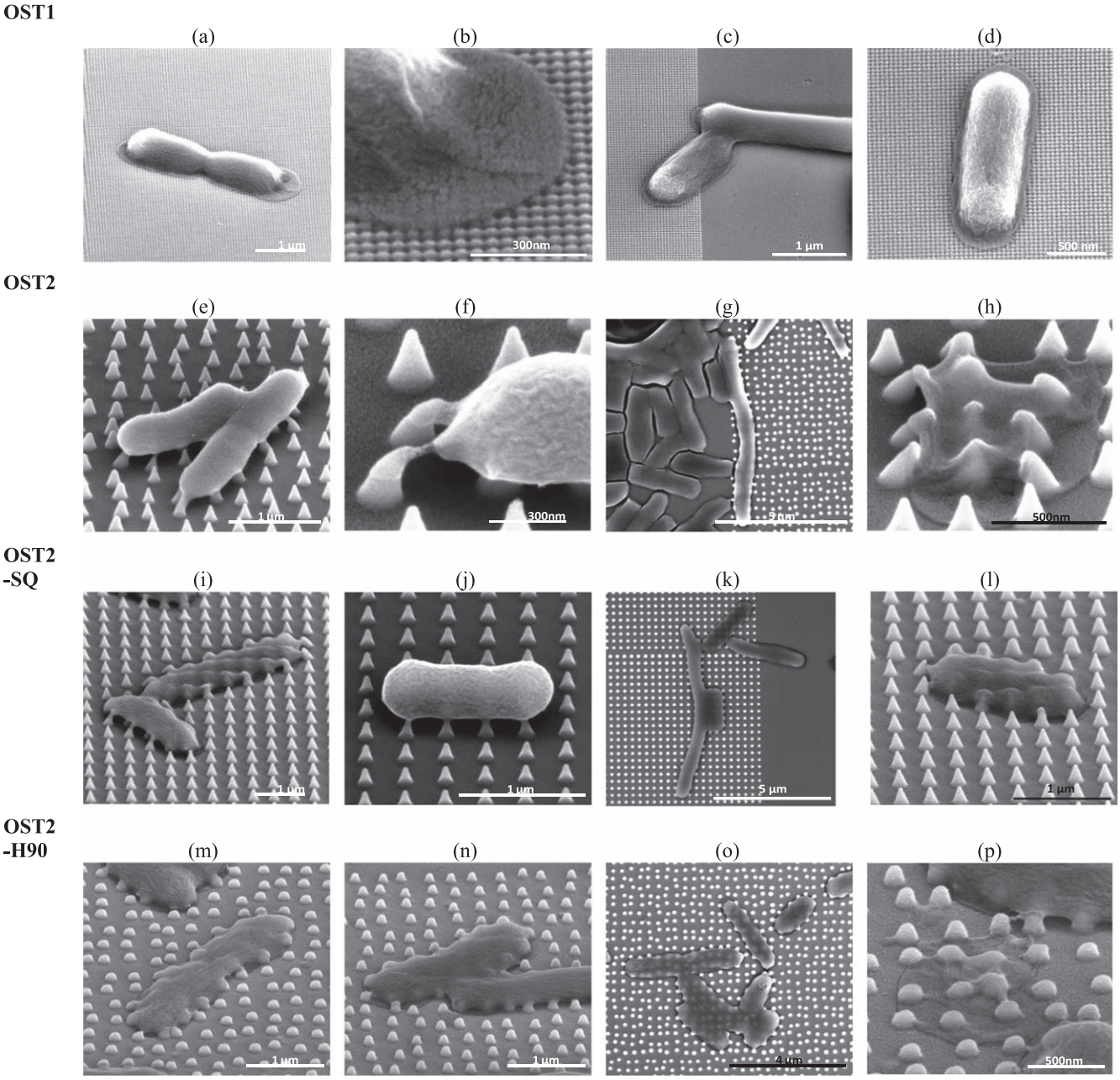

Figure 2. SEM images of the *E. coli* cell-nanopattern interface: (a)–(d) OST1; (e)–(h) OST2; (i)–(l) OST2-SQ; (m–p) OST2-H90.

figure 2(g)), deformed rod shapes (wrinkled cells due to contact with the nanopillars), and completely deflated cells (figure 2(h)). Very large cell lengths suggest that the cells were stressed and, thus, could not divide [6, 29]. The EPS secreted by these cells was generally present at the tip of the nanopillars only (figure 2(f)). The EPS seemed to have been stretched to reach the disordered nanopillars. Moreover, some of the nanopillars in contact with the cells were bent (figures 2(e), (f), (h)). As opposed to OST1, where no damaged cells were detected, 13.5 ± 7% of the bacteria were damaged on the surfaces patterned with OST2 nanopatterns (figure 3(d)). Such severe cell damage is associated with death of *E. coli* (and other motile bacteria), as previously shown by SEM and live/dead investigations [17, 30, 31]. Although extremely large cell lengths were observed for OST2, the mean cell length was not significantly different from OST1 (figure 3(a)). There were however, cells significantly narrower (figure 3(b)) and the amount of EPS was significantly lower for OST2 (figure 3(c)) as compared to OST1. These changes further confirm the abnormal cell morphology and limited cell-surface contact that were qualitatively described above.

The response of the cells to OST2-SQ surfaces was compared with OST2 to study the effects of controlled disorder on the bactericidal behavior of OST2. Controlled disorder has been previously shown to benefit osteogenic differentiation of MSCs as opposed to the ordered square arrangement, which preserved the stemness of the MSCs [20]. It was therefore important to investigate whether this controlled disorder plays any role in the response of *E. coli* cells to the nanopatterns. The ratio of damaged cells to the total

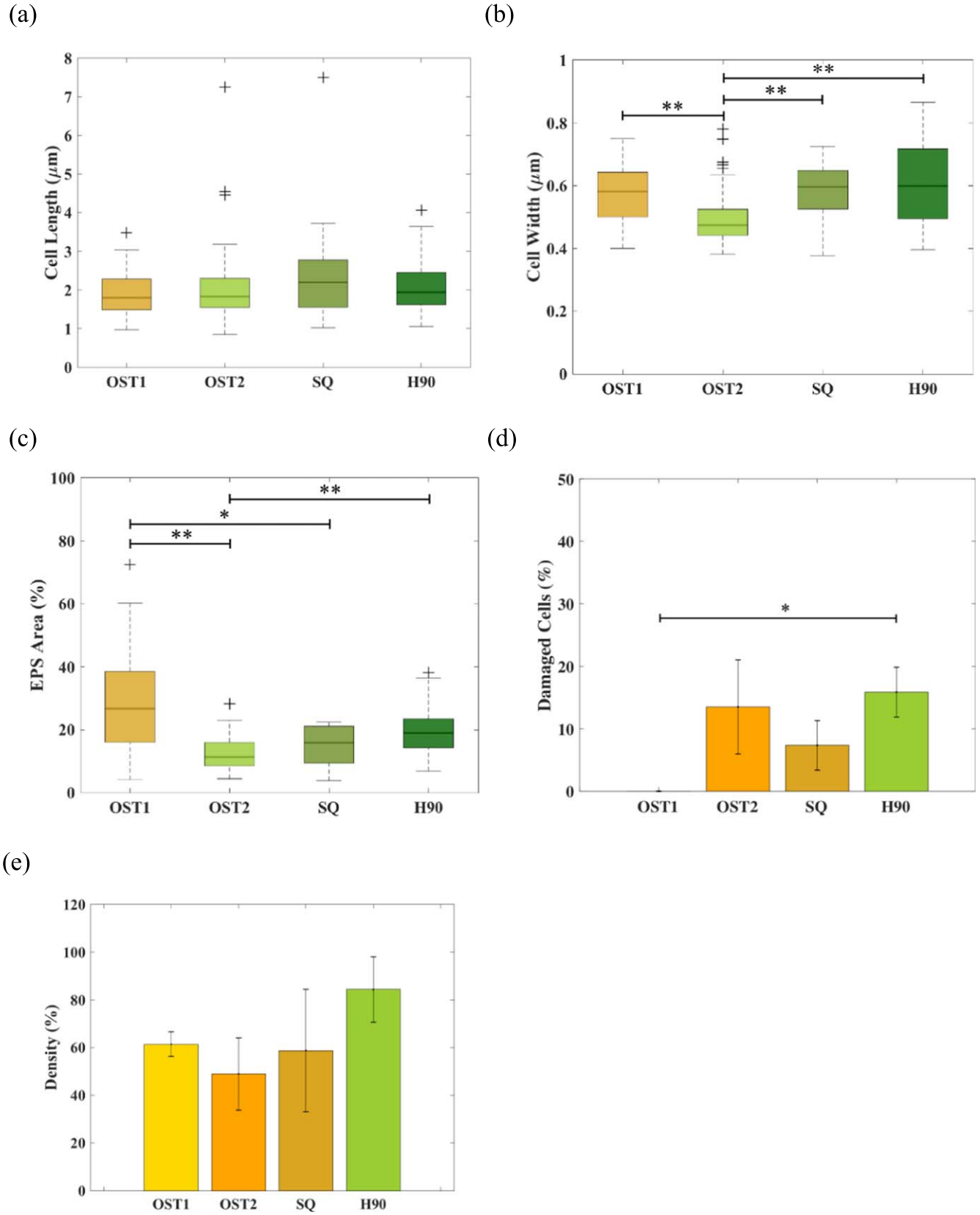

Figure 3. Quantitative characterization of *E. coli* cells attached on the nanopatterns: (a) cell length; (b) cell width; (c) area of the extracellular polymeric substance (EPS); (d) damaged cells; (e) cell density relative to the non-patterned area. (a)–(c) are box plots. (d) and (e) are bar plots with mean and standard deviation. (* $p < 0.05$; ** $p < 0.01$).

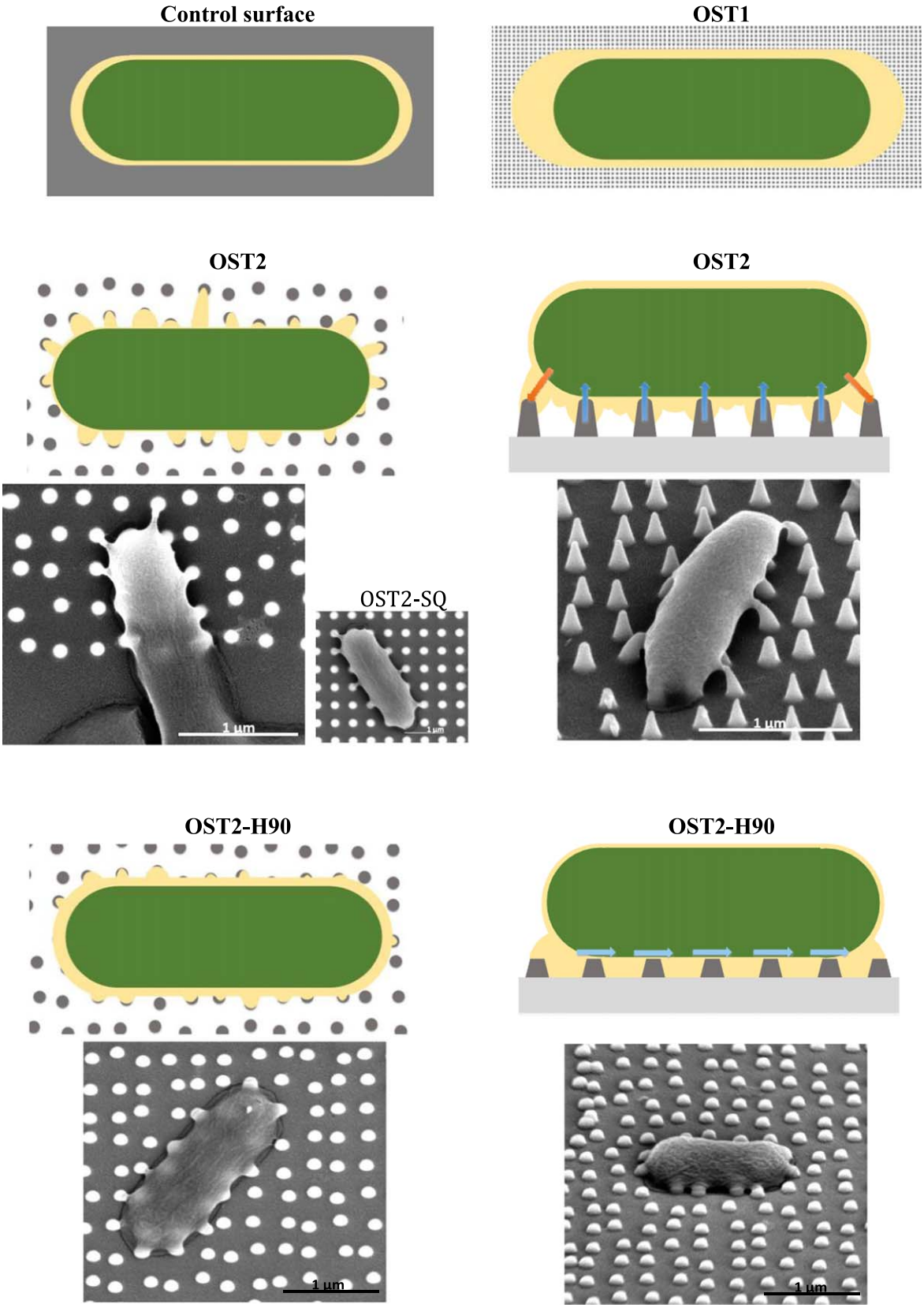

Figure 4. Schematics and SEM images (top and side views) of the cell-nanopillar interface showing the EPS distribution on the control (non-patterned) surfaces, OST1, OST2 and OST2-H90 nanopatterns.

number of cells was not significantly different between OST2 and OST2-SQ (figure 3(d)). This indicates that controlled disorder, which is known to benefit osteogenicity, does not adversely affect the bactericidal effects of these surfaces. Very large cells were also occasionally observed for OST2-SQ (figure 2(k)), while there was no significant difference in the mean cell length as compared to both OST1 and OST2 (figure 3(a)). The amount of EPS and cell density on OST2-SQ were also similar to the case of OST2 (figures 3(c), (e)). The mean width of the cells was, however, somewhat higher on OST2-SQ as compared to OST2, suggesting a healthier less-stressed state of the cells (figure 3(b)). This observation together with the numerically (but statistically insignificant) higher values of the ratio of the damaged cells in the case of OST2 (figure 3(d)) hints that controlled disorder may be even beneficial for inducing antibacterial effects.

Natural and biomimetic nanopatterns with bactericidal effects often possess high-aspect ratios with heights of ≈200 nm or larger [5–7] while osteogenic effects have been usually reported for shorter pillars (i.e.<100 nm) [1–4]. We therefore produced another group of nanopatterns (OST-H90) whose features were similar to OST2 except for the height of the nanopillars, which was about half of what was used in OST2. Cells could adhere well on this surface and showed a well-spread EPS around the cell body and in between the nanopillars (figures 2(m)–(p)). No stressed cells with very large lengths were observed (figure 3(a)). The mean cell length was also not different from the other groups. The width of the cells (figure 3(b)) as well as the amount of EPS (figure 3(c)) were somewhat higher for this group and comparable with that of OST1. However, the bactericidal effects continued to be present with many adhered cells showing flat or leaked morphologies (figure 2(p)) and with a ratio of damaged cells that was not significantly different from OST2 or OST2-SQ (figure 3(d)).

The mechanisms behind the cellular responses observed here need to be further investigated. The EPS, which is a nonspecific adhesin used by *E. coli* to attach to surfaces [32], was present on all nanopatterns but showed different surface distributions (figure 4). While in the case of non-patterned areas and OST1 (with small and dense nanopillars), the EPS could extend freely on the surface around the cell body, it was observed mainly at the tip of the nanopillars for OST2 and OST2-SQ. In the case of OST2-H90, EPS was visible both on and in between the nanopillars (figure 4). Furthermore, the EPS seemed to have been stretched more on the OST2 surfaces to reach the disordered nanopillars than on the OST2-SQ (figure 4, OST2-SQ inset). These observations suggest that cells on the investigated nanopatterns may experience different local stresses during attachment and movement, which could play a role in the cellular responses observed. Antibacterial mechanisms proposed so far, by which nanopatterns induce bacterial cell death include physical damage and rupture of the cell wall layers [5, 7, 10] and generation of reactive oxygen species with effects on vital cellular functions [33]. Mechanistic studies at the single cell level are required to investigate the nanopattern-induced cell death. These studies should consider the role of nanopattern features, EPS, cell type and properties, cell temporal changes during attachment (adaptability) as well as the biomechanics of cell-nanopattern interfaces [11, 31, 34]. Based on these studies, rational design criteria can be established for antibacterial nanopatterns.

As mentioned earlier, two major challenges when trying to prolong the longevity of orthopedic implants are enhanced osseointegration [35, 36] and prevention of implant-associated infections [37–39]. Nanopatterns that could simultaneously address both challenges are therefore very welcome additions to the arsenal of tools available for satisfying these demands. In that sense, the findings of this study support a new paradigm for development of instructive biomaterials based on multifunctional nanopatterns. The nanopatterns of this study should be further tested for osteogenic potential and for maximizing the two biofunctionalities. From a technological viewpoint, EBID provides unparalleled possibilities in terms of accurate and reproducible fabrication of nanopatterns with arbitrary shapes, dimensions, and arrangements on flat and curved surfaces [40–42]. These enable systematic mechanistic studies based on which well-defined nanopatterns can be found for specific biofunctionalities. However, scaling up the amount of surfaces covered by nanopatterns requires further developments of the process for example by using multibeam systems and by combining EBID with such techniques as nanolithography [40] and nanoimprinting [43, 44]. That would allow (pre-)clinical testing of these patterns.

4. Conclusions

We showed for the first time here that controlled nanopatterns produced by EBID and having features derived from osteogenic ones (e.g. interspace, controlled disorder) could exhibit bactericidal properties for *E. coli*. In addition, the study demonstrates the feasibility of EBID as an enabling nanotechnology for these applications. Therefore, these findings pave the way towards the development of (multi)functional nanopatterns for not only bone implants.

ORCID iDs

Peter-Leon Hagedoorn https://orcid.org/0000-0001-6342-2022
Cornelis W Hagen https://orcid.org/0000-0002-0973-9886
Lidy E Fratila-Apachitei https://orcid.org/0000-0002-7341-4445

References

[1] Albrektsson T and Johansson C 2001 Osteoinduction, osteoconduction and osseointegration *Eur. Spine. J.* **10** S96–101

[2] Dobbenga S, Fratila-Apachitei L E and Zadpoor A A 2016 Nanopattern-induced osteogenic differentiation of stem cells–a systematic review *Acta Biomater.* **46** 3–14

[3] Silverwood R K, Fairhurst P G, Sjöström T, Welsh F, Sun Y, Li G, Yu B, Young P S, Su B and Meek R 2016 Analysis of osteoclastogenesis/osteoblastogenesis on nanotopographical titania surfaces *Adv. Healthcare Mater.* **5** 947–55

[4] Sjöström T, Dalby M J, Hart A, Tare R, Oreffo R O and Su B 2009 Fabrication of pillar-like titania nanostructures on titanium and their interactions with human skeletal stem cells *Acta Biomater.* **5** 1433–41

[5] Bandara C D, Singh S, Afara I O, Wolff A, Tesfamichael T, Ostrikov K and Oloyede A 2017 Bactericidal effects of natural nanotopography of dragonfly wing on *Escherichia coli ACS Appl. Mater. Interfaces* **9** 6746–60

[6] Dickson M N, Liang E I, Rodriguez L A, Vollereaux N and Yee A F 2015 Nanopatterned polymer surfaces with bactericidal properties *Biointerphases* **10** 021010

[7] Ivanova E P, Hasan J, Webb H K, Truong V K, Watson G S, Watson J A, Baulin V A, Pogodin S, Wang J Y and Tobin M J 2012 Natural bactericidal surfaces: mechanical rupture of pseudomonas aeruginosa cells by cicada wings *Small* **8** 2489–94

[8] Teo B K K, Wong S T, Lim C K, Kung T Y, Yap C H, Ramagopal Y, Romer L H and Yim E K 2013 Nanotopography modulates mechanotransduction of stem cells and induces differentiation through focal adhesion kinase *ACS Nano* **7** 4785–98

[9] Yim E K, Darling E M, Kulangara K, Guilak F and Leong K W 2010 Nanotopography-induced changes in focal adhesions, cytoskeletal organization, and mechanical properties of human mesenchymal stem cells *Biomaterials* **31** 1299–306

[10] Linklater D P, Juodkazis S, Rubanov S and Ivanova E P 2017 Comment on 'Bactericidal effects of natural nanotopography of dragonfly wing on *Escherichia coli*' *ACS Appl. Mater. Interfaces* **9** 29387–93

[11] Cao Y, Su B, Chinnaraj S, Jana S, Bowen L, Charlton S, Duan P, Jakubovics N S and Chen J 2018 Nanostructured titanium surfaces exhibit recalcitrance towards *Staphylococcus epidermidis* biofilm formation *Sci. Rep.* **8** 1071

[12] Dalby M J, Gadegaard N and Oreffo R O 2014 Harnessing nanotopography and integrin–matrix interactions to influence stem cell fate *Nat. Mater.* **13** 558

[13] Nikukar H, Reid S, Tsimbouri P M, Riehle M O, Curtis A S and Dalby M J 2013 Osteogenesis of mesenchymal stem cells by nanoscale mechanotransduction *ACS Nano* **7** 2758–67

[14] Sjöström T, McNamara L E, Meek R, Dalby M J and Su B 2013 2D and 3D nanopatterning of titanium for enhancing osteoinduction of stem cells at implant surfaces *Adv. Healthcare Mater.* **2** 1285–93

[15] Yang J, McNamara L E, Gadegaard N, Alakpa E V, Burgess K V, Meek R D and Dalby M J 2014 Nanotopographical induction of osteogenesis through adhesion, bone morphogenic protein cosignaling, and regulation of microRNAs *ACS Nano* **8** 9941–53

[16] Wang N, Tytell J D and Ingber D E 2009 Mechanotransduction at a distance: mechanically coupling the extracellular matrix with the nucleus *Nat. Rev. Mol. Cell Biol.* **10** 75

[17] Tsimbouri P M, Fisher L, Holloway N, Sjostrom T, Nobbs A H, Meek R M D, Su B and Dalby M J 2016 Osteogenic and bactericidal surfaces from hydrothermal titania nanowires on titanium substrates *Sci. Rep.* **6** 1–12

[18] Janbaz S, Noordzij N, Widyaratih D S, Hagen C W, Fratila-Apachitei L E and Zadpoor A A 2017 Origami lattices with free-form surface ornaments *Sci. Adv.* **3** eaao1595

[19] Wnuk J, Rosenberg S, Gorham J, Van Dorp W, Hagen C and Fairbrother D 2011 Electron beam deposition for nanofabrication: insights from surface science *Surf. Sci.* **605** 257–66

[20] Dalby M J, Gadegaard N, Tare R, Andar A, Riehle M O, Herzyk P, Wilkinson C D and Oreffo R O 2007 The control of human mesenchymal cell differentiation using nanoscale symmetry and disorder *Nat. Mater.* **6** 997

[21] Kantawong F, Burgess K E, Jayawardena K, Hart A, Burchmore R J, Gadegaard N, Oreffo R O and Dalby M J 2009 Whole proteome analysis of osteoprogenitor differentiation induced by disordered nanotopography and mediated by ERK signalling *Biomaterials* **30** 4723–31

[22] Tsimbouri P M, Murawski K, Hamilton G, Herzyk P, Oreffo R O, Gadegaard N and Dalby M J 2013 A genomics approach in determining nanotopographical effects on MSC phenotype *Biomaterials* **34** 2177–84

[23] Wang J R, Ahmed S F, Gadegaard N, Meek R D, Dalby M J and Yarwood S J 2014 Nanotopology potentiates growth hormone signalling and osteogenesis of mesenchymal stem cells *Growth Hormone IGF Res.* **24** 245–50

[24] Utke I, Hoffmann P and Melngailis J 2008 Gas-assisted focused electron beam and ion beam processing and fabrication *J. Vac. Sci. Technol.* B **26** 1197–276

[25] Yavas O, Ochiai C, Takai M, Park Y, Lehrer C, Lipp S, Frey L, Ryssel H, Hosono A and Okuda S 2000 Field emitter array fabricated using focused ion and electron beam induced reaction *J. Vac. Sci. Technol.* B **18** 976–9

[26] Botman A, Mulders J J L and Hagen C W 2009 Creating pure nanostructures from electron-beam-induced deposition using purification techniques: a technology perspective *Nanotechnology* **20** 372001

[27] Hirt L, Reiser A, Spolenak R and Zambelli T 2017 Additive manufacturing of metal structures at the micrometer scale *Adv. Mater.* **29** 1604211

[28] Plank H, Gspan C, Dienstleder M, Kothleitner G and Hofer F 2008 The influence of beam defocus on volume growth rates for electron beam induced platinum deposition *Nanotechnology* **19** 485302

[29] Meel C, Kouzel N, Oldewurtel E R and Maier B 2012 Three-dimensional obstacles for bacterial surface motility *Small* **8** 530–4

[30] Ivanova E P *et al* 2013 Bactericidal activity of black silicon *Nat. Commun.* **4** 1–7

[31] Diu T, Faruqui N, Sjöström T, Lamarre B, Jenkinson H F, Su B and Ryadnov M G 2014 Cicada-inspired cell-instructive nanopatterned arrays *Sci. Rep.* **4** 7122

[32] Renner L D and Weibel D B 2011 Physicochemical regulation of biofilm formation *MRS Bull.* **36** 347–55

[33] Sahoo S, Krishnamurthy Rao K, Suresh A and Suraishkumar G 2004 Intracellular reactive oxygen species mediate suppression of sporulation in Bacillus subtilis under shear stress *Biotechnol. Bioeng.* **87** 81–9

[34] Hasan J, Webb H K, Truong V K, Pogodin S, Baulin V A, Watson G S, Watson G A, Crawford R J and Ivanova E P 2013 Selective bactericidal activity of nanopatterned superhydrophobic cicada Psaltoda claripennis wing surfaces *Appl. Microbiol. Biotechnol.* **97** 9257–62

[35] Ma Q-L, Zhao L-Z, Liu R-R, Jin B-Q, Song W, Wang Y, Zhang Y-S, Chen L-H and Zhang Y-M 2014 Improved implant osseointegration of a nanostructured titanium surface via mediation of macrophage polarization *Biomaterials* **35** 9853–67

[36] Raphel J, Holodniy M, Goodman S B and Heilshorn S C 2016 Multifunctional coatings to simultaneously promote osseointegration and prevent infection of orthopaedic implants *Biomaterials* **84** 301–14

[37] Amin Yavari S, Loozen L, Paganelli F L, Bakhshandeh S, Lietaert K, Groot J A, Fluit A C, Boel C, Alblas J and Vogely H C 2016 Antibacterial behavior of additively manufactured porous titanium with nanotubular surfaces releasing silver ions *ACS Appl. Mater. Interfaces* **8** 17080–9

[38] Bakhshandeh S, Gorgin Karaji Z, Lietaert K, Fluit A C, Boel C E, Vogely H C, Vermonden T, Hennink W E, Weinans H and Zadpoor A A 2017 Simultaneous delivery of multiple antibacterial agents from additively manufactured porous biomaterials to fully eradicate planktonic and adherent staphylococcus aureus *ACS Appl. Mater. Interfaces* **9** 25691–9

[39] van Hengel I A, Riool M, Fratila-Apachitei L E, Witte-Bouma J, Farrell E, Zadpoor A A, Zaat S A and Apachitei I 2017 Selective laser melting porous metallic implants with immobilized silver nanoparticles kill and prevent biofilm formation by methicillin-resistant staphylococcus aureus *Biomaterials* **140** 1–15

[40] Guan Y, Fowlkes J D, Retterer S T, Simpson M L and Rack P D 2008 Nanoscale lithography via electron beam induced deposition *Nanotechnology* **19** 505302

[41] Schirmer M, Walz M M, Vollnhals F, Lukasczyk T, Sandmann A, Chen C, Steimruck H P and Marbach H 2011 Electron-beam-induced deposition and post-treatment processes to locally generate clean titanium oxide nanostructures on Si(100) *Nanotechnology* **22** 085301

[42] Riazanova A V, Costanzi B N, Aristov A I, Rikers Y G M, Mulders J J L, Kabashin A V, Dahlaberg E D and Belova L M 2016 Gas-assisted electron-beam-induced nanopatterning of high-quality titanium oxide *Nanotechnology* **27** 115304

[43] Ahn S, Cha J, Myung H, Kim S-M and Kang S 2006 Continuous ultraviolet roll nanoimprinting process for replicating large-scale nano-and micropatterns *Appl. Phys. Lett.* **89** 213101

[44] Ahn S H and Guo L J 2009 Large-area roll-to-roll and roll-to-plate nanoimprint lithography: a step toward high-throughput application of continuous nanoimprinting *ACS Nano* **3** 2304–10